
BIOBLOBS: Differentiable Graph Partitioning for Protein Representation Learning

Xin Wang^{1,2}, Carlos Oliver¹

¹Vanderbilt University, Nashville, Tennessee, USA

²Yale University, New Haven, Connecticut, USA

Abstract

Protein function is driven by coherent substructures which vary in size and topology, yet current protein representation learning models (PRL) distort these signals by relying on rigid substructures such as k -hop and fixed radius neighbourhoods. We introduce BIOBLOBS, a plug-and-play, fully differentiable module that represents proteins by dynamically partitioning structures into flexibly-sized, non-overlapping substructures (“blobs”). The resulting blobs are quantized into a shared and interpretable codebook, yielding a discrete vocabulary of function-relevant protein substructures used to compute protein embeddings. We show that BIOBLOBS’s representations improve the performance of widely used protein encoders such as GVP-GNN across various PRL tasks. Our approach highlights the value of architectures that directly capture function-relevant protein substructures, enabling both improved predictive performance and mechanistic insight into protein function. Source code is available at <https://github.com/OliverLaboratory/BioBlobs>

1 Introduction

Proteins are structured macromolecules that drive fundamental biological processes across the tree of life. A protein’s ability to carry out its function is rooted in its specific three-dimensional arrangement—its fold. Despite decades of painstaking curation and experimentation revealing many ways in which folds mediate biological processes, the vast majority of proteins in major databases remain without reliable functional annotation (Kustatscher et al., 2022).

For a long time, a key obstacle to assigning function was the difficulty of determining the structure for a given sequence. This bottleneck has been alleviated by highly accurate structure predictors such as the AlphaFold Jumper et al. (2021) and ESM (Lin et al., 2023) families, yielding databases with hundreds of millions of predicted structures. With structures now broadly available, the central challenge is to encode structural information at this unprecedented scale.

Protein representation learning (PRL) (Wu et al., 2022) addresses this by training neural models to capture salient structural and biophysical properties in compact embeddings that can inform downstream tasks. Given a protein, PRL methods typically proceed in two stages: (1) choose a basic “atom” or unit (e.g., a sequence span, a residue with its nearest neighbours, a voxel, or a secondary-structure element); and (2) encode each unit in the context of the whole to produce a final representation. These representations feed decoders for supervised tasks (e.g., binding-site detection, pathway membership, protein–protein interaction prediction, protein design) Gligorijević et al. (2021); Derry et al. (2025); Watson et al. (2023); Dauparas et al. (2022), or are learned via self-supervision to produce general-purpose encodings Zhang et al. (2022); Chen et al. (2024).

Existing PRL systems often operate over rigidly defined units (Fasoulis et al., 2021), yet protein function is driven by cohesive substructures that operate modularly (Rorick & Wagner, 2011).

Among many examples are catalytic triads (Ser–His–Asp), Rossmann-like nucleotide-binding cores, and P-loop (Walker A/B) NTPase sites (Dodson & Wlodawer, 1998; Rossmann et al., 1974; Leipe et al., 2003). When the unit is fixed *a priori*—e.g., k -hop neighbourhoods or voxel grids—models can fracture functional assemblies and distort the learned representations. This would be like trying to understand the mechanisms of a bicycle by cutting it into uniformly sized cubes. Likewise in proteins, functional modules rarely adopt such regular substructures. Compounding this, the appropriate units are context-dependent and vary in size and topology. Moreover, the atomization step is inherently discrete (e.g., selecting a residue and its neighbours), making it non-differentiable and therefore typically excluded from end-to-end training. The atoms we seek should be (1) connected substructures of the protein, (2) contributory to function, and (3) distributed modularly, reflecting the conservative forces of evolution.

We cast the problem of atomising a protein into cohesive substructures as a graph-partitioning task (Buluç et al., 2016). Protein graphs—capturing neighbourhood relations and spatial organisation among residues or atoms—are standard in PRL, with GVP-GNNs being a widely used example (Jing et al., 2021). Graph partitioning assigns each node to exactly one part, producing a disjoint cover of the graph; on residue/atom graphs, such partitions yield non-overlapping groups—precisely the structural units we aim to model. Because the space of partitions grows exponentially with the number of nodes, many natural formulations are NP-hard (Feder et al., 1999). Nonetheless, recent advances in neural combinatorial optimisation over graphs learn probability distributions on nodes/edges to construct powerful probabilistic algorithms for tasks such as set cover, alignment, and compression (Karalias & Loukas, 2020; Bouritsas et al., 2021). These ideas remain largely unexplored within PRL.

Here we propose BIOBLOBS, which performs principled partitioning of 3D protein graphs into cohesive substructures.

- **Neural partitioning layer for PRL.** We introduce BIOBLOBS, a plug-and-play neural graph-partitioning layer that represents proteins as learnable functions of their **coherent substructure units**, guarantees connectivity, adapts granularity to the task, and can be placed atop established encoders (e.g., standard GNNs and GVP-based models). Parameter sharing enables the model to distil recurring substructures, reflecting the natural modularity of proteins.
- **Strong empirical performance.** BIOBLOBS achieves top performance on three established protein-function benchmarks under rigorous controls for structure leakage, outperforming strong PRL baselines.
- **Ablations on granularity.** We systematically vary the maximum substructure size and the number of partitions, providing insight into organisational principles of protein structure and function.
- **Interpretability.** Importance scores over discovered substructures enable higher-order interpretability, linking predictions to human-understandable functional units.

2 BIOBLOBS

The BIOBLOBS layer dynamically computes a hard assignment of residues to distinct substructures (sets of residues) which we term “blobs”. We then compute representations of each blob and incorporate global context to arrive at a final embedding for the whole protein.

2.1 Protein Graph Construction

We represent each protein structure as a geometric graph $\mathcal{G} = (\mathcal{V}, \mathcal{E})$, where nodes $v_i \in \mathcal{V}$ correspond to amino acid residues and edges $(i, j) \in \mathcal{E}$ connect residues that are spatially proximate, determined by the k -nearest neighbors of the C_α coordinates. Each node v_i is associated with geometric features $\mathbf{h}_i = (\mathbf{s}_i, \mathbf{V}_i)$, derived from the coordinates of the O, C, C_α, N atoms in the residue. These features consist of scalar components $\mathbf{s}_i \in \mathbb{R}^{d_s}$ (e.g., dihedral angles) and vector components $\mathbf{V}_i \in \mathbb{R}^{d_v \times 3}$ (e.g., orientations). Similarly, each edge is assigned features $\mathbf{h}_{ij}^E = (\mathbf{s}_{ij}, \mathbf{V}_{ij})$, where $\mathbf{s}_{ij} \in \mathbb{R}^{d_e}$ denotes scalar values such as inter-residue distances, and $\mathbf{V}_{ij} \in \mathbb{R}^{d_{ev} \times 3}$ represents vector quantities such as spatial directions.

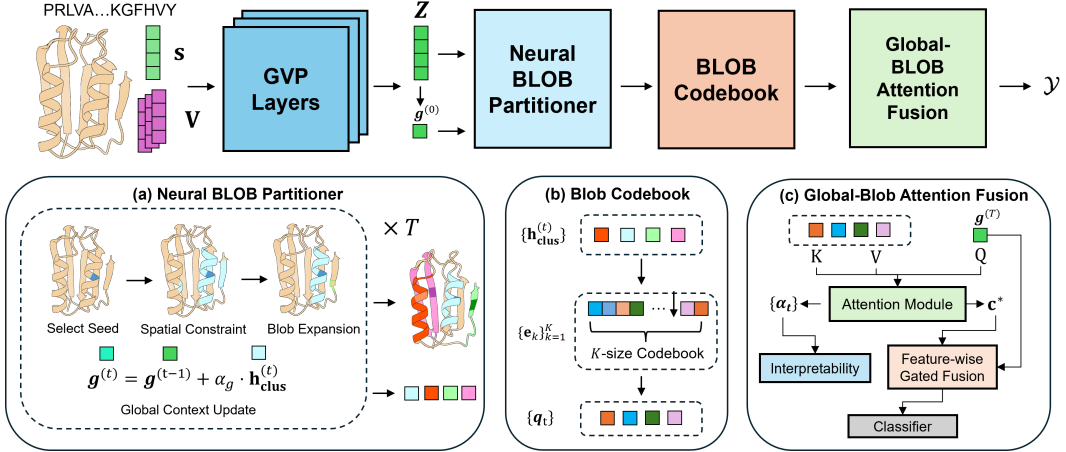


Figure 1: Overview of the BIOBLOBS pipeline. The framework consists of four main components: a protein encoder, a neural partitioner, a blob codebook, and a global-blob attention fusion module. The GVP encoder first processes the protein graph and produces residue embeddings. **(a) Neural BLOB Partitioner.** A seed residue is first selected with Gumbel–Softmax. Its k -hop neighborhood is then identified to restrict the candidate pool. Finally, a blob expander scores the candidates and assigns residues to form cohesive local substructures. **(b) Blob Codebook.** The resulting blob embeddings are quantized into a discrete codebook that captures frequent and label-relevant protein substructures. **(c) Global-BLOB Attention Fusion.** The quantized blob embeddings are integrated with the global feature using a multi-key attention mechanism. This produces both a fused representation for classification and an interpretable importance score distribution over blobs.

2.2 Protein Structure Encoder

We employ Geometric Vector Perceptron (GVP) layers (Jing et al., 2021) to obtain initial residue-level features while preserving geometric equivariance. The structure encoder consists of L GVP convolution layers:

$$\mathbf{h}_i^{(\ell+1)} = \text{GVPConv} \left(\mathbf{h}_i^{(\ell)}, \left\{ \mathbf{h}_j^{(\ell)} : j \in \mathcal{N}(i) \right\}, \mathbf{h}_{ij}^E \right) \quad (1)$$

where $\mathcal{N}(i)$ denotes the neighbors of node i . After L layers, we obtain updated scalar node features through a projection layer, $\mathbf{z}_i = \text{Proj} \left(\mathbf{s}_i^{(L)} \right) \in \mathbb{R}^D$, which are then used to guide the partition module.

2.3 Neural BLOB Partitioner

Given residue embeddings $\mathbf{Z} = [\mathbf{z}_1, \dots, \mathbf{z}_N] \in \mathbb{R}^{N \times D}$ for a protein with N residues, we first derive an initial global context vector $\mathbf{g}^{(0)}$ by pooling all residue embeddings. The partitioner then constructs up to T blobs through an iterative differentiable process. Initially, we create an assignment matrix $\mathbf{M}^{(0)} \in \{0, 1\}^{N \times T}$, which records the residue composition of each blob at iteration $t \in [1, 2, \dots, T]$. An availability mask $\mathbf{m}^{(0)} \in \{0, 1\}^N$ is also maintained to keep track of unassigned residues and prevent overlapping assignments. At each iteration $t > 0$, we proceed discrete, differentiable partition (Bouritsas et al., 2021) with three key steps.

Seed Residue Selection. We begin by using a seed scoring network to predict logits over all residues: $\ell^{(t)} = f_{\text{seed}}([\mathbf{Z}; \mathbf{g}^{(t-1)}]) \in \mathbb{R}^N$. Unavailable residues are masked by setting their logits to $-\infty$ using $\mathbf{m}^{(t-1)}$, ensuring that only unassigned residues remain candidates. We then sample from a relaxed categorical distribution using Gumbel–Softmax (Jang et al., 2016):

$$\mathbf{w}^{(t)} = \text{softmax} \left(\frac{\tilde{\ell}^{(t)} + \mathbf{n}}{\tau^{(t)}} \right), \quad \eta_i \sim \text{Gumbel}(0, 1), \quad (2)$$

where the temperature $\tau^{(t)} = \max(\tau_{\min}, \tau_{\text{init}} \cdot \gamma^t)$ gradually decreases, shifting the sampling from exploratory to more deterministic behavior during training. To obtain a discrete seed while retaining gradients, we apply the straight-through (ST) estimator (Bengio et al., 2013):

$$\begin{aligned} \mathbf{e}^{(t)} &= \text{one_hot}\left(\arg \max_i w_i^{(t)}\right), & \tilde{\mathbf{w}}^{(t)} &= \mathbf{e}^{(t)} + (\mathbf{w}^{(t)} - \text{sg}(\mathbf{w}^{(t)})), \\ \mathbf{z}_{\text{seed}}^{\text{ST}} &= \sum_{i=1}^N \tilde{w}_i^{(t)} \mathbf{z}_i. \end{aligned} \quad (3)$$

In the forward pass, the hard one-hot vector $\mathbf{e}^{(t)}$ is used as the actual seed. In the backward pass, $\mathbf{w}^{(t)}$ is substituted so that gradients flow into the seed scorer and encoder. The straight-through seed embedding $\mathbf{z}_{\text{seed}}^{\text{ST}}$ thus acts as a continuous proxy for the discrete seed, enabling the partitioner to remain differentiable while still capturing the semantics of hard residue assignment.

Threshold Prediction. Given the seed residue $v_{\text{seed}}^{(t)}$, we derive its k -hop neighborhood and restrict to available residues $\mathcal{R}^{(t)} = \mathcal{N}_k(v_{\text{seed}}^{(t)}; \mathcal{E}) \cap \mathbf{m}^{(t-1)}$, which serves as the candidate set for expansion. A learned threshold head then predicts a per-blob threshold $\theta^{(t)}$ using the straight-through seed embedding \mathbf{z}_{seed} , the global context $\mathbf{g}^{(t-1)}$, and local structural statistics $\phi^{(t)}$ computed over $\mathcal{R}^{(t)}$:

$$\theta^{(t)} = f_{\text{thresh}}([\mathbf{z}_{\text{seed}}^{\text{ST}}; \mathbf{g}^{(t-1)}; \phi^{(t)}]), \quad (4)$$

This threshold adaptively controls how many candidates are included, thereby regulating the blob size in the subsequent expansion step.

Blob Expansion. Given the threshold $\theta^{(t)}$ and the candidate set $\mathcal{R}^{(t)}$, we expand around the seed by computing seed-conditioned scores, turning them into probabilities, forming straight-through hard memberships, and pooling a blob embedding that updates the global context.

$$s_i^{(t)} = \frac{(\mathbf{W}_k^{\text{Part}} \mathbf{z}_i) \cdot (\mathbf{W}_q^{\text{Part}} \mathbf{z}_{\text{seed}}^{\text{ST}})}{\sqrt{d}}, \quad v_i \in \mathcal{R}^{(t)}. \quad (5)$$

We map each score to an inclusion probability with a temperature-scaled sigmoid $p_i^{(t)}$, thresholded at 0.5 to obtain a binary membership $c_i^{(t)}$, and use a straight-through correction $\tilde{p}_i^{(t)}$ so gradients pass through the soft probability. To prevent a blob from growing unbounded, we further impose a maximum size S , keeping only the top- S candidates ranked by their inclusion probabilities.

$$p_i^{(t)} = \sigma((s_i^{(t)} - \theta^{(t)})/\tau^{(t)}), \quad c_i^{(t)} = \mathbb{I}[p_i^{(t)} \geq 0.5], \quad \tilde{p}_i^{(t)} = c_i^{(t)} + (p_i^{(t)} - \text{sg}(p_i^{(t)})) \quad (6)$$

To obtain a differentiable blob representation while keeping discrete selection in the forward pass, we use a straight-through blob embedding that combines a hard mean and a soft mean as

$$\mathbf{h}_{\text{hard}}^{(t)} = \frac{\sum_i c_i^{(t)} \mathbf{z}_i}{\sum_i c_i^{(t)} + \varepsilon}, \quad \mathbf{h}_{\text{soft}}^{(t)} = \frac{\sum_i \tilde{p}_i^{(t)} \mathbf{z}_i}{\sum_i \tilde{p}_i^{(t)} + \varepsilon}, \quad \mathbf{h}_{\text{clus}}^{(t)} = \mathbf{h}_{\text{hard}}^{(t)} + (\mathbf{h}_{\text{soft}}^{(t)} - \text{sg}(\mathbf{h}_{\text{soft}}^{(t)})).$$

This straight-through form ensures that the forward computation uses the discrete blob for interpretability, while gradients flow through the soft weights to update the scorer and the encoder. The global context is updated in residual form, $\mathbf{g}^{(t+1)} = \mathbf{g}^{(t)} + \alpha_g f_{\text{global}}(\mathbf{h}_{\text{clus}}^{(t)})$, which accumulates information from discovered blobs without overwriting prior context and stabilizes training via the step size α_g . Finally, $\mathbf{M}^{(t)}$ is updated according to the new blob partition. A concise step-by-step procedure is given in Algorithm 1.

2.4 Substructure Codebook

After the partitioner, we obtain blob embeddings $\mathbf{H} = [\mathbf{h}_{\text{clus}}^{(1)}, \dots, \mathbf{h}_{\text{clus}}^{(T)}] \in \mathbb{R}^{T \times D}$. We introduce a vector-quantization codebook $\mathbf{E} = \{\mathbf{e}_k\}_{k=1}^K \subset \mathbb{R}^D$ to map each blob to a discrete substructure token (Van Den Oord et al., 2017; Razavi et al., 2019), steering the encoder and partitioner to discover

function-relevant substructures shared across the dataset. Let \mathbf{h}_t denote the t -th blob embedding, the nearest-neighbor quantization selects its token as

$$k_t = \arg \min_{k \in \{1, \dots, K\}} \|\mathbf{h}_t - \mathbf{e}_k\|_2^2, \quad \mathbf{q}_t = \mathbf{e}_{k_t}. \quad (7)$$

We use the standard straight-through estimator so the forward pass uses the quantized vector while gradients update the encoder. To keep blob embeddings close to their selected codes, we use a commitment loss with stop-gradient from VQ-VAE-2 (Razavi et al., 2019). Besides, we add an entropy regularizer based on code usage probabilities $\{p_k\}_{k=1}^K$ to discourage dead codes and promote diverse usage:

$$\mathcal{L}_{\text{commit}} = \beta \sum_{t=1}^T \|\mathbf{h}_t - \text{sg}(\mathbf{q}_t)\|_2^2. \quad \mathcal{L}_{\text{ent}} = \lambda_{\text{ent}} \sum_{k=1}^K p_k \log\left(\frac{p_k}{1/K}\right). \quad (8)$$

The code vectors are updated by an exponential moving average (EMA) during training, as shown in Appendix C.1. The codebook outputs the quantized substructure representations form $\mathbf{H}_q = [\mathbf{q}_1, \dots, \mathbf{q}_T] \in \mathbb{R}^{T \times D}$.

2.5 Global-Blob Attention Fusion

Finally, we integrate the quantized blob embeddings with the global protein representation using a single-query, multi-key attention mechanism (Vaswani et al., 2017), where $\mathbf{g} = \mathbf{g}^{(T)}$ serves as the query and \mathbf{H}_q provides keys and values. We first project the query, keys, and values, and compute attention weights over blobs:

$$\mathbf{q} = \mathbf{W}_q \mathbf{g}, \quad \mathbf{K} = \mathbf{W}_k \mathbf{H}_q, \quad \mathbf{V} = \mathbf{W}_v \mathbf{H}_q, \quad \pi = \text{softmax}\left(\frac{\mathbf{q}^\top \mathbf{K}}{\sqrt{D}}\right). \quad (9)$$

The weights $\pi \in \mathbb{R}^T$ act as importance scores, indicating the relative contribution of each blob to the global representation. The weighted blob summary is then

$$\mathbf{c}^* = \mathbf{V} \pi \in \mathbb{R}^D, \quad (10)$$

which allows the global context to attend to informative substructures. Finally, we fuse the global feature and the blob summary with a feature-wise gate:

$$\mathbf{h}_{\text{fuse}} = \text{LN}(\mathbf{g} + \beta \odot \mathbf{W}_{\text{fuse}} \mathbf{c}^*), \quad \beta = \sigma(\text{MLP}([\mathbf{g}; \mathbf{c}^*])), \quad (11)$$

where $\mathbf{W}_{\text{fuse}} \in \mathbb{R}^{D \times D}$ is a linear projection. The gate $\beta \in (0, 1)^D$ adaptively balances the contributions of global features pooled from residue embeddings and local signals from the Blobs, and the fused representation \mathbf{h}_{fuse} is passed to the classifier for prediction.

2.6 Time Complexity Analysis

The full pipeline after the protein encoder runs in near-linear time with respect to the number of residues. Among the components, the Neural Partitioner contributes the main cost, while the sub-structure codebook and global-blob attention add only modest overhead.

Neural Partitioner. Let $\mathcal{G} = (\mathcal{V}, \mathcal{E})$ denote the protein graph with $N = |\mathcal{V}|$ residues and $|\mathcal{E}| = O(k_{\text{NN}} N)$ edges, where k_{NN} is the number of neighbors used in the k -nearest neighbor construction of the graph. The partitioner builds up to T blobs through the iterative seed-threshold-expansion process, where k_{hop} controls the radius of the neighborhood explored around each seed. At each iteration, three steps dominate the cost:

- (i) *Seed selection:* the scorer computes logits over all N residues and applies Gumbel-Softmax sampling, which is linear in the number of nodes, $O(N)$.
- (ii) *Neighborhood construction:* the k_{hop} -hop neighborhood of the seed is obtained through a sparse traversal, which touches up to k_{hop} layers of edges and costs $O(k_{\text{hop}} |\mathcal{E}|)$.
- (iii) *Blob expansion:* each candidate in the neighborhood is scored by a seed-conditioned dot product, converted into probabilities, and thresholded, which again requires linear work in the number of candidates, bounded by $O(N)$.

Thus, the per-iteration complexity is $O(k_{\text{hop}} |\mathcal{E}| + N)$, and over T iterations the total becomes

$$O(T(k_{\text{hop}} |\mathcal{E}| + N)) = O(T(k_{\text{hop}} k_{\text{NN}} + 1) N). \quad (12)$$

Substructure Codebook. For each of the T blob embeddings with dimension D , the codebook computes squared distances to all K code vectors. This requires $O(TKD)$ time, followed by nearest-neighbor assignment and an EMA update of the selected codes. Both operations share the same order of complexity, so quantization remains linear in the number of blobs and codes.

Global-Blob Attention. The fusion step integrates the global protein context with the T blob embeddings. Projecting queries, keys, and values has cost $O((N + T)D^2)$, but since these projections are reused and D is fixed, the dominant term is the attention operation itself. Computing attention scores across T blobs with H heads requires $O(THD)$, followed by weighted pooling and a feature-wise gating step in $O(D^2)$. Because $T \ll N$ and H is fixed, the fusion module is lightweight compared to the partitioner.

2.7 Multi-Stage Training

We adopt a two-stage training scheme to optimize BIOBLOBS in a stable and efficient manner.

- **Stage 1:** We first train the encoder, partitioner, and global-blob attention fusion while bypassing the substructure codebook. The original blob embeddings are used for fusion. This stage allows the model to form meaningful blobs relevant to protein function using only the cross-entropy loss.
- **Stage 2:** We initialize the codebook using K -means clustering on the blob embeddings learned in Stage 1, providing well-separated starting codes. The fusion module receives the quantized blob embeddings as input. The codebook is then unfrozen for end-to-end optimization, where the commitment and entropy losses are introduced alongside classification. The weights of these codebook-related losses are gradually ramped to stabilize convergence and balance discrete representation learning with predictive performance.

This progressive strategy preserves predictive performance in Stage 1, while reducing training instability and enabling the codebook to capture frequent substructures in Stage 2.

3 Experiments

In this section, we present experiments designed to evaluate BIOBLOBS across diverse protein prediction tasks, highlighting its ability to generalize under both functional and structural challenges.

Datasets ProteinShake (Kucera et al., 2023) is a benchmarking toolkit that offers ready-to-use protein structure datasets, splits, and metrics across many tasks. We selected **Gene Ontology(GO)**, **EC (Enzyme Commission)**, and **Structural Class(SCOP)** to evaluate our method. In the GO dataset, we predict only the *Molecular Function* branch, where each label denotes a molecular-level activity a protein can perform (e.g., binding or catalysis), making this a multi-label task. For the EC dataset, the label is a top-level EC class that groups enzymes by reaction chemistry, such as oxidoreductases, forming a multi-class task. For the SCOP dataset, we predict *SCOP-FA*, where labels capture families defined by shared three-dimensional fold and evolutionary relatedness, again as a multi-class task focused on fold/family recognition. Across all three datasets, we evaluate under both a random split and a structure split. The structure split clusters proteins by structural similarity and assigns clusters to different splits to reduce leakage, and we use a 0.7 similarity threshold to separate closely related structures, following ProteinShake experiments. Dataset statistics are displayed in Table 1.

Table 1: Details on Benchmark Datasets

Dataset	# Proteins	Area of protein biology	Metric
Gene Ontology (GO)	32,633	Functions, Components, Pathways	F_{max}
Enzyme Commission (EC)	15,603	Reaction catalysis	Accuracy
Structural class (SCOP)	10,066	Geometric relationships	Accuracy

Baselines and Implementations We benchmark **GNN**, a naïve **GVP-GNN**, and **GVP+DiffPool** against two stages of BIOBLOBS. GIN follows the ProteinShake baseline on residue graphs with

a task-matched classifier. The naïve GVP-GNN shares the same GVP encoder as BIOBLOBS but applies graph-level pooling over residue embeddings for classification. GVP-GNN serves as a backbone baseline to show the added value of BIOBLOBS’s architecture. DiffPool provides a comparison to learned soft clustering: after the GVP encoder, a single DiffPool layer assigns residues to clusters, then one pass of cluster-level message passing and fusion with residue features yields predictions. For BIOBLOBS, we keep hyperparameters fixed across datasets and split strategies to avoid over-tuning and to highlight robustness. Specifically, we use the same protein structure encoder as GVP-GNN, and we cap the number of blobs $T = 5$ and the blob size at $S = 15$ for neural partitioner to balance training efficiency and accuracy. We report test results for Stage 1 (BIOBLOBS w/o codebook) and Stage 2 (BIOBLOBS) to quantify the contribution of each BIOBLOBS’ component. The hyperparameter settings for BIOBLOBS are reported in Appendix B.1.

Table 2: Comparison of models trained with different representations of protein structure across various tasks, evaluated on both **random** and **structure-based** data splits. Shown are mean and standard deviation across four runs with different seeds.

Representation	Split	SCOP-FA	Enzyme Class	Gene Ontology
GNN	Random	0.495 ± 0.012	0.790 ± 0.007	0.704 ± 0.001
	Structure	0.415 ± 0.015	0.621 ± 0.026	0.474 ± 0.014
GVP-GNN	Random	0.4663 ± 0.001	0.801 ± 0.004	0.569 ± 0.032
	Structure	0.464 ± 0.027	0.451 ± 0.003	0.504 ± 0.004
GVP+DiffPool	Random	0.312 ± 0.013	0.807 ± 0.005	0.583 ± 0.001
	Structure	0.264 ± 0.022	0.657 ± 0.004	0.458 ± 0.016
BIOBLOBS w/o Codebook	Random	0.495 ± 0.009	0.823 ± 0.013	0.669 ± 0.001
	Structure	0.442 ± 0.001	0.671 ± 0.012	0.525 ± 0.001
BIOBLOBS	Random	0.506 ± 0.002	0.840 ± 0.001	0.817 ± 0.001
	Structure	0.467 ± 0.007	0.684 ± 0.004	0.528 ± 0.003

3.1 Protein Classification Performance

According to Table 2, BIOBLOBS is best on all three datasets under both *random* and *structure* splits, with larger margins on the structure split that limits similarity leakage. On EC (structure), the score rises from 0.621 for GNN to 0.684 with BIOBLOBS (**+10%**) and from 0.451 for GVP-GNN to 0.684 (**+52%**). Notably, BIOBLOBS without the codebook surpasses GVP-GNN on EC and GO, indicating that the neural partitioner and the global–cluster attention fusion help the model target function-relevant local substructures instead of averaging signals over the full graph. Adding the codebook then gives further gains without hurting classification despite quantization: a VQ-VAE-style straight-through path with EMA updates and a commitment term steers blob embeddings toward a compact, reusable set of frequent, function-related patterns; on GO (random), the score increases from 0.669 to 0.817 (**+22%**).

GVP-GNN does not reliably outperform GNN. For the EC’s structure split, it drops to 0.451 versus 0.621 for GNN, likely because global pooling dilutes signals from small active sites. Integrating DiffPool with GVP-GNN does not consistently improve over the baselines because one-shot soft coarsening can merge residues that are spatially distant or functionally unrelated into the same cluster. This blending weakens the functional signal of true substructures and introduces noise in the form of irrelevant or misleading features that distract the classifier. BIOBLOBS avoids these issues by growing compact local blobs with the neural partitioner and fusing them with a light attention gate, which reduces noise from disconnected parts and sharpens label alignment.

3.2 BioBlobs Partition Interpretation

We offer initial analysis of the model’s partitions by visualizing its blobs on proteins from the EC test set (structure split) using ChimeraX (Fig. 2). For structurally similar proteins like 1GBX and 1JUG, BIOBLOBS appears to consistently identify well-defined secondary structures in similar regions, such as α -helices and β -sheets, which shows its robustness in finding function-relevant substructures. The model’s importance scores further improve this interpretability. High scores are assigned

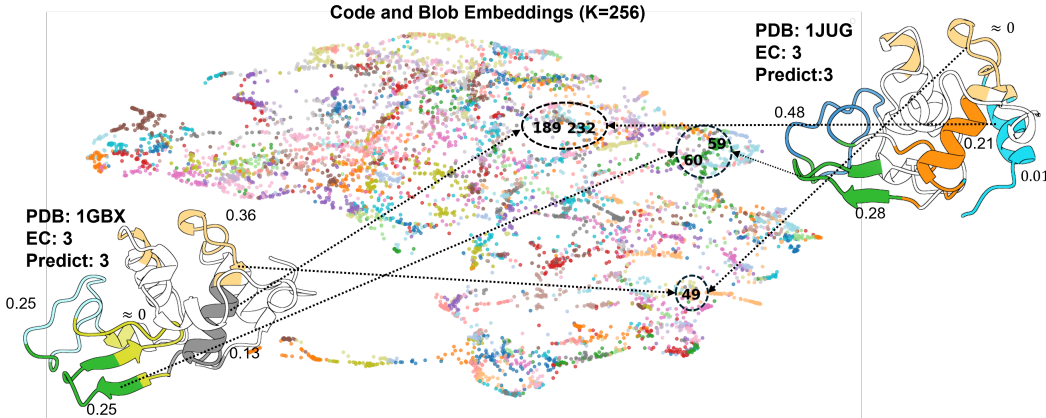


Figure 2: UMAP projection of the blob and code embeddings for the EC(structure) test set, where code embeddings are marked by their indices. Example BIOBLOBS partitions are shown on two sides. Colored regions represent distinct blobs and their code index. Each protein is annotated with its PDB ID, true and predicted EC numbers, and the importance score π_t for each blob.

to coherent, stable structures while lower scores are given to disconnected regions, indicating that the model learns to prioritize key structural motifs. Finally, the codebook provides insight by mapping structurally similar blobs to the same or nearby codes. For example, a light orange motif in both proteins is quantized to code 49, while their green β -sheets map to the adjacent codes 59 and 60. Similarly, α -helices in both proteins map to the nearby codes 189 and 232. This demonstrates that the codebook learns a meaningful and consistent vocabulary for protein substructures. Therefore, we show that BIOBLOBS provides a robust and interpretable bridge between a protein’s 3D structure and its learned, function-relevant substructures. The complete UMAP for blob and cluster embedding is shown in the Appendix C. This preliminary analysis motivates that future work should focus on systematic analysis of BIOBLOBS importance scores and properties of learned substructures.

3.3 Neural Partitioner Case Study

In Fig. 3, we study how the neural partitioner parameters influence the test performance of BIOBLOBS on the EC and SCOP-FA datasets. We focus on two factors: the maximum blob size S and the maximum number of blobs T , while keeping other hyperparameters fixed. For maximum blob size, we fix $T = 5$. The left figure shows that increasing S from 5 to 15 gives slight performance improvements, but pushing it further to 25 causes a clear drop. This suggests that both datasets benefit from substructures of moderate size (5–10 residues), whereas overly large blobs tend to merge unrelated residues, thereby diluting function-specific signals and reducing accuracy. For the number of blobs, we fix $S = 15$. The right figure shows a similar pattern across datasets. Accuracy peaks when only five blobs are used, then declines as more blobs are introduced, likely because additional, function-irrelevant blobs compete for attention and confuse the classifier. Interestingly, when $T = 25$, the performance rebounds. At this point, nearly all residues are assigned to blobs, which raises the chance of covering function-relevant substructures and improves prediction. Overall, both “how many” and “how large” the blobs are should accommodate the specific protein predictive task. When labels depend on short, localized motifs (for example, catalytic or binding patches), a maximum blob size of 10–15 is effective. When labels depend on domain-level organization, a larger cap around 25 may help.

4 Related Work

Protein Structure Modeling Protein GNNs typically build residue-level graphs (distance or k -NN) and pass messages; equivariant backbones such as GVP remain strong. Higher-order lifts via simplicial/cell-complex networks capture multi-body interactions (Bodnar et al., 2021; Goh et al., 2022; Wang et al., 2025), and surface-centric models learn directly on molecular surfaces from MaSIF onward (Gainza et al., 2020). We also adopt residue graphs, but go beyond fixed neigh-

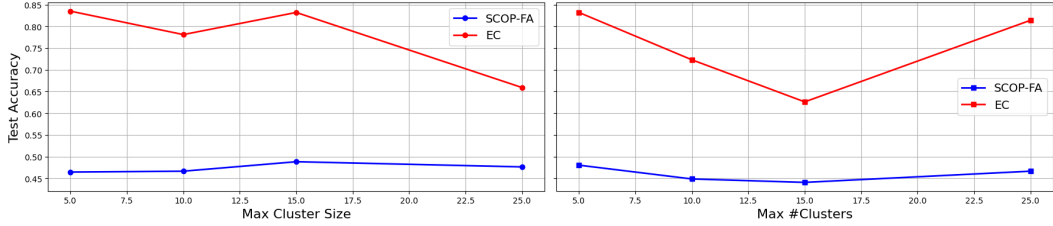


Figure 3: Neural partitioner case study: tuning maximum cluster size S and number of clusters T .

borhoods with learned, connected substructures that are quantized via a codebook to better match modular organization.

Protein Motifs and Substructures Protein function is often mediated by recurrent modules such as catalytic triads, Rossmann cores, and P-loop NTPase sites (Dodson & Wlodawer, 1998; Rossmann et al., 1974; Leipe et al., 2003). Domain-scale taxonomies (SCOPe, CATH) catalog such units and are standard for supervision and leakage control (Chandonia et al., 2022; Orengo et al., 1997). Our approach targets finer, task-adaptive, connected ‘‘blobs’’ and quantizes them into a reusable substructure vocabulary.

Graph Pooling, Subgraphs, and Partitioning Graph pooling coarsens graphs via soft assignments/selections (DiffPool, MinCutPool, Graph U-Nets/Top-K, SAGPool, ASAP) (Liu et al., 2022), while subgraph GNNs rely on rigid extraction (Alsentzer et al., 2020). In contrast, *partitioning* assigns each node to exactly one cluster under constraints; many formulations are NP-hard (Feder et al., 1999), motivating learned relaxations and neural combinatorial methods (Karalias & Loukas, 2020; Bouritsas et al., 2021). Our layer is a differentiable partitioner for proteins: it selects seeds with straight-through Gumbel sampling and expands connected blobs within bounded neighborhoods to yield non-overlapping, size-controlled substructures.

Discrete Representation Learning Discrete latents turn continuous features into tokens: VQ-VAE with commitment/ST losses and its variants (VQ-VAE-2, VQGAN) connect to product/residual quantization (Van Den Oord et al., 2017; Razavi et al., 2019). Protein-specific discretization (e.g., Foldseek’s alphabet) shows the value of tokenized 3D patterns (Van Kempen et al., 2024). We quantize learned blob embeddings with EMA/commitment/entropy regularization, yielding an interpretable substructure lexicon fused via global–blob attention.

5 Conclusion

BIOBLOBS is a deep protein-structure representation framework that dynamically captures the modular organization of proteins. We address the challenge of selecting substructures of variable size and topology by introducing a differentiable seed-and-expand procedure for connected node sets, coupled with discrete codebook (vector-quantized) learning. Across three protein-property prediction benchmarks, BIOBLOBS combined with GVP-based feature extractors consistently outperforms strong baselines. Together, these results lay a foundation for more faithful protein representations and a scalable, systematic account of structure–function relationships.

References

Emily Alsentzer, Samuel Finlayson, Michelle Li, and Marinka Zitnik. Subgraph neural networks. *Advances in Neural Information Processing Systems*, 33:8017–8029, 2020.

Yoshua Bengio, Nicholas Léonard, and Aaron Courville. Estimating or propagating gradients through stochastic neurons for conditional computation. *arXiv preprint arXiv:1308.3432*, 2013.

Cristian Bodnar, Fabrizio Frasca, Nina Otter, Yuguang Wang, Pietro Lio, Guido F Montufar, and Michael Bronstein. Weisfeiler and lehman go cellular: Cw networks. *Advances in neural information processing systems*, 34:2625–2640, 2021.

Giorgos Bouritsas, Andreas Loukas, Nikolaos Karalias, and Michael Bronstein. Partition and code: learning how to compress graphs. *Advances in Neural Information Processing Systems*, 34:18603–18619, 2021.

Aydn Buluç, Henning Meyerhenke, Ilya Safro, Peter Sanders, and Christian Schulz. Recent advances in graph partitioning. *Algorithm engineering: selected results and surveys*, pp. 117–158, 2016.

John-Marc Chandonia, Lindsey Guan, Shiangyi Lin, Changhua Yu, Naomi K Fox, and Steven E Brenner. Scope: improvements to the structural classification of proteins—extended database to facilitate variant interpretation and machine learning. *Nucleic acids research*, 50(D1):D553–D559, 2022.

Dexiong Chen, Philip Hartout, Paolo Pellizzoni, Carlos Oliver, and Karsten Borgwardt. Endowing protein language models with structural knowledge. *arXiv preprint arXiv:2401.14819*, 2024.

Justas Dauparas, Ivan Anishchenko, Nathaniel Bennett, Hua Bai, Robert J Ragotte, Lukas F Milles, Basile IM Wicky, Alexis Courbet, Rob J de Haas, Neville Bethel, et al. Robust deep learning-based protein sequence design using proteinmpnn. *Science*, 378(6615):49–56, 2022.

Alexander Derry, Alp Tartici, and Russ B Altman. Protein functional site annotation using local structure embeddings. *Proceedings of the National Academy of Sciences*, 122(34):e2513219122, 2025.

G. Dodson and A. Wlodawer. Catalytic triads and their relatives. *Trends in Biochemical Sciences*, 23(9):347–352, 1998. doi: 10.1016/S0968-0004(98)01254-7.

Romanos Fasoulis, Georgios Paliouras, and Lydia E Kavraki. Graph representation learning for structural proteomics. *Emerging Topics in Life Sciences*, 5(6):789–802, 2021.

Tomas Feder, Pavol Hell, Sulamita Klein, and Rajeev Motwani. Complexity of graph partition problems. In *Proceedings of the thirty-first annual ACM symposium on Theory of computing*, pp. 464–472, 1999.

Pablo Gainza, Freyr Sverrisson, Frederico Monti, Emanuele Rodola, Davide Boscaini, Michael M Bronstein, and Bruno E Correia. Deciphering interaction fingerprints from protein molecular surfaces using geometric deep learning. *Nature methods*, 17(2):184–192, 2020.

Vladimir Gligorijević, P Douglas Renfrew, Tomasz Kosciolek, Julia Koehler Leman, Daniel Berenberg, Tommi Vatanen, Chris Chandler, Bryn C Taylor, Ian M Fisk, Hera Vlamakis, et al. Structure-based protein function prediction using graph convolutional networks. *Nature communications*, 12(1):3168, 2021.

Christopher Wei Jin Goh, Cristian Bodnar, and Pietro Lio. Simplicial attention networks. *arXiv preprint arXiv:2204.09455*, 2022.

Eric Jang, Shixiang Gu, and Ben Poole. Categorical reparameterization with gumbel-softmax. *arXiv preprint arXiv:1611.01144*, 2016.

Bowen Jing, Stephan Eismann, Patricia Suriana, Raphael J. L. Townshend, and Ron Dror. Learning from Protein Structure with Geometric Vector Perceptrons, May 2021. URL <http://arxiv.org/abs/2009.01411>. arXiv:2009.01411 [q-bio].

John Jumper, Richard Evans, Alexander Pritzel, Tim Green, Michael Figurnov, Olaf Ronneberger, Kathryn Tunyasuvunakool, Russ Bates, Augustin Žídek, Anna Potapenko, et al. Highly accurate protein structure prediction with alphafold. *nature*, 596(7873):583–589, 2021.

Nikolaos Karalias and Andreas Loukas. Erdos goes neural: an unsupervised learning framework for combinatorial optimization on graphs. *Advances in Neural Information Processing Systems*, 33: 6659–6672, 2020.

Tim Kucera, Carlos Oliver, Dexiong Chen, and Karsten Borgwardt. Proteinshake: Building datasets and benchmarks for deep learning on protein structures. In *Advances in Neural Information Processing Systems 36 (NeurIPS 2023) — Datasets and Benchmarks Track*, pp. 58277–58289, 2023. URL https://proceedings.neurips.cc/paper_files/paper/2023/hash/b6167294ed3d6fc61e11e1592ce5cb77-Paper-Datasets_and_Benchmarks.pdf.

Georg Kustatscher, Tom Collins, Anne-Claude Gingras, Tiannan Guo, Henning Hermjakob, Trey Ideker, Kathryn S Lilley, Emma Lundberg, Edward M Marcotte, Markus Ralser, et al. Understudied proteins: opportunities and challenges for functional proteomics. *Nature Methods*, 19(7): 774–779, 2022.

Dmitry D. Leipe, Eugene V. Koonin, and L. Aravind. Evolution and classification of p-loop kinases and NTPases. *Journal of Molecular Biology*, 333(4):781–815, 2003. doi: 10.1016/j.jmb.2003.08.031.

Zeming Lin, Halil Akin, Roshan Rao, Brian Hie, Zhongkai Zhu, Wenting Lu, Nikita Smetanin, Robert Verkuil, Ori Kabeli, Yaniv Shmueli, et al. Evolutionary-scale prediction of atomic-level protein structure with a language model. *Science*, 379(6637):1123–1130, 2023.

Chuang Liu, Yibing Zhan, Jia Wu, Chang Li, Bo Du, Wenbin Hu, Tongliang Liu, and Dacheng Tao. Graph pooling for graph neural networks: Progress, challenges, and opportunities. *arXiv preprint arXiv:2204.07321*, 2022.

Christine A Orengo, Alex D Michie, Susan Jones, David T Jones, Mark B Swindells, and Janet M Thornton. Cath—a hierarchic classification of protein domain structures. *Structure*, 5(8):1093–1109, 1997.

Ali Razavi, Aaron Van den Oord, and Oriol Vinyals. Generating diverse high-fidelity images with vq-vae-2. *Advances in neural information processing systems*, 32, 2019.

Mary M Rorick and Günter P Wagner. Protein structural modularity and robustness are associated with evolvability. *Genome biology and evolution*, 3:456–475, 2011.

Michael G. Rossmann, Dino Moras, and Kenneth W. Olsen. Chemical and biological evolution of a nucleotide-binding protein. *Nature*, 250:194–199, 1974. doi: 10.1038/250194a0.

Aaron Van Den Oord, Oriol Vinyals, et al. Neural discrete representation learning. *Advances in neural information processing systems*, 30, 2017.

Michel Van Kempen, Stephanie S Kim, Charlotte Tumescheit, Milot Mirdita, Jeongjae Lee, Cameron LM Gilchrist, Johannes Söding, and Martin Steinegger. Fast and accurate protein structure search with foldseek. *Nature biotechnology*, 42(2):243–246, 2024.

Ashish Vaswani, Noam Shazeer, Niki Parmar, Jakob Uszkoreit, Llion Jones, Aidan N Gomez, Łukasz Kaiser, and Illia Polosukhin. Attention is all you need. *Advances in neural information processing systems*, 30, 2017.

Zhiyu Wang, Arian Jamasb, Mustafa Hajij, Alex Morehead, Luke Braithwaite, and Pietro Liò. Topotein: Topological deep learning for protein representation learning. *arXiv preprint arXiv:2509.03885*, 2025.

Joseph L Watson, David Juergens, Nathaniel R Bennett, Brian L Trippe, Jason Yim, Helen E Eisenach, Woody Ahern, Andrew J Borst, Robert J Ragotte, Lukas F Milles, et al. De novo design of protein structure and function with rfdiffusion. *Nature*, 620(7976):1089–1100, 2023.

Lirong Wu, Yufei Huang, Haitao Lin, and Stan Z Li. A survey on protein representation learning: Retrospect and prospect. *arXiv preprint arXiv:2301.00813*, 2022.

Zuobai Zhang, Minghao Xu, Arian Jamasb, Vijil Chenthamarakshan, Aurelie Lozano, Payel Das, and Jian Tang. Protein representation learning by geometric structure pretraining. *arXiv preprint arXiv:2203.06125*, 2022.

A Appendix

Use of Large Language Models (LLMs)

LLMs were used to assist in coding, writing, and producing figures. All LLM-produced code and text was thoroughly double-checked.

B Reproducibility

All code, data, and weights necessary to reproduce results and use our models on new data are available on <https://github.com/OliverLaboratory/BioBlobs>. Benchmarking was done with the ProteinShake Kucera et al. (2023) open source library to ensure reproducibility.

B.1 Model Hyperparameters

Default Hyperparameters. We summarize the default hyperparameters used in the two-stage training of BIOBLOBS across 3 datasets and 2 splits.

Stage 1 (baseline training). We train the encoder, partitioner, and global-cluster attention fusion for 120 epochs with batch size 128 and learning rate 10^{-3} . The GVP encoder uses scalar–vector input dimensions of $(6, 3)$ for residues and $(32, 1)$ for edges, with hidden dimensions $(100, 16)$ and $(32, 1)$, respectively. We stack three GVP convolution layers with dropout rate 0.1 and apply sum pooling for graph readout. The neural partitioner is configured with up to $T = 5$ clusters, hidden dimension 50, $k = 1$ hop expansion, maximum cluster size 15, termination threshold 0.95, and temperature annealing from $\tau_{\text{init}} = 1.0$ to $\tau_{\text{min}} = 0.1$ with exponential decay 0.95.

Stage 2 (joint training with codebook). We resume from the Stage 1 checkpoint and initialize the substructure codebook using K –means clustering on the pre-trained cluster embeddings. The codebook has 256 entries of dimension 100 (matching the scalar hidden dimension) and is updated by EMA with decay 0.99. Training continues for 30 epochs with reduced learning rate 10^{-4} and without backbone freezing. Additional objectives are introduced: the commitment loss with weight $\lambda_{\text{vq}} = 1.0$ and the entropy regularizer with $\lambda_{\text{ent}} = 0.1$. This staged procedure allows the encoder and partitioner to first stabilize on meaningful blobs, after which the codebook is optimized jointly without destabilizing the backbone.

B.2 Neural Blob Partitioner Algorithm

Algorithm 1 Neural BLOB Partitioner

Require: Residue embeddings $\mathbf{Z} \in \mathbb{R}^{N \times D}$, edge index \mathcal{E} , max blobs T , max blob size S , k -hop radius k , temperature schedule $\{\tau^{(t)}\}$, termination threshold ρ , step size α_g

Ensure: Assignment $\mathbf{M} \in \{0, 1\}^{N \times T}$, blob embeddings $\mathbf{H} = [\mathbf{h}_{\text{clus}}^{(1)}, \dots, \mathbf{h}_{\text{clus}}^{(T)}]$

1: $\mathbf{g}^{(0)} \leftarrow \text{Pool}(\mathbf{Z})$; $\mathbf{M} \leftarrow \mathbf{0}$; $\mathbf{m} \leftarrow \mathbf{1}_N$ ▷ global context, assignment, availability

2: **for** $t = 1$ to T **do**

3: **Early stop:** if $\text{coverage}(\mathbf{M}) \geq \rho$ or no i with $m_i = 1$, **break**

4: **Seed selection**

5: $\ell^{(t)} \leftarrow f_{\text{seed}}([\mathbf{Z}; \mathbf{g}^{(t-1)}])$; mask unavailable: $\tilde{\ell}^{(t)} = \ell^{(t)} + \log \mathbf{m}$

6: $\mathbf{w}^{(t)} \leftarrow \text{GumbelSoftmax}(\tilde{\ell}^{(t)}, \tau^{(t)})$ ▷ hard variant with straight-through (ST)

7: $\mathbf{e}^{(t)} \leftarrow \text{one_hot}(\arg \max_i w_i^{(t)})$; $\tilde{\mathbf{w}}^{(t)} \leftarrow \mathbf{e}^{(t)} + (\mathbf{w}^{(t)} - \text{sg}(\mathbf{w}^{(t)}))$

8: $\mathbf{z}_{\text{seed}}^{\text{ST}} \leftarrow \sum_i \tilde{w}_i^{(t)} \mathbf{z}_i$; $i_s \leftarrow \arg \max_i e_i^{(t)}$

9: $\mathbf{M}[i_s, t] \leftarrow 1$; $m_{i_s} \leftarrow 0$

10: **Candidate set and local stats**

11: $\mathcal{R}^{(t)} \leftarrow \mathcal{N}_k(i_s; \mathcal{E}) \cap \{i : m_i = 1\}$ ▷ k -hop and available

12: $\phi^{(t)} \leftarrow \text{LocalStats}(\mathcal{R}^{(t)})$ ▷ log#cands, seed-link fraction, induced density

13: **Threshold prediction**

14: $\theta^{(t)} \leftarrow f_{\text{thresh}}([\mathbf{z}_{\text{seed}}^{\text{ST}}; \mathbf{g}^{(t-1)}; \phi^{(t)}])$

15: **Blob expansion**

16: For $i \in \mathcal{R}^{(t)}$: $s_i^{(t)} = \frac{(\mathbf{W}_k \mathbf{z}_i)^\top (\mathbf{W}_q \mathbf{z}_{\text{seed}}^{\text{ST}})}{\sqrt{d}}$ ▷ optionally add normalized link term

17: $p_i^{(t)} = \sigma((s_i^{(t)} - \theta^{(t)}) / \tau^{(t)})$; $c_i^{(t)} = \mathbb{I}[p_i^{(t)} \geq 0.5]$ ▷ ST hard gate

18: Keep the seed and the top- S residues by $p_i^{(t)}$; set other $c_i^{(t)} = 0$

19: For all i : $\mathbf{M}[i, t] \leftarrow c_i^{(t)}$; $m_i \leftarrow m_i \cdot (1 - c_i^{(t)})$

20: **Blob embedding (ST) and context update**

21: $\mathbf{h}_{\text{hard}}^{(t)} = \frac{\sum_i c_i^{(t)} \mathbf{z}_i}{\sum_i c_i^{(t)} + \varepsilon}$, $\mathbf{h}_{\text{soft}}^{(t)} = \frac{\sum_i \tilde{p}_i^{(t)} \mathbf{z}_i}{\sum_i \tilde{p}_i^{(t)} + \varepsilon}$, $\mathbf{h}_{\text{clus}}^{(t)} = \mathbf{h}_{\text{hard}}^{(t)} + (\mathbf{h}_{\text{soft}}^{(t)} - \text{sg}(\mathbf{h}_{\text{soft}}^{(t)}))$

22: $\mathbf{g}^{(t)} \leftarrow \mathbf{g}^{(t-1)} + \alpha_g f_{\text{global}}(\mathbf{h}_{\text{clus}}^{(t)})$

23: **end for**

24: **return** \mathbf{M}, \mathbf{H}

C Codebook and Blob Embedding Visualization

We obtain blob embeddings before quantization and compare them with code embeddings extracted from the codebook. Using UMAP, we visualize both on the EC test set under random and structure splits, where red integers mark the positions of code embeddings. In the structure split, code embeddings appear more densely packed and form clearer clusters compared to the random split. This aligns with the fact that the structure split places structurally similar proteins (0.7) in the test set.

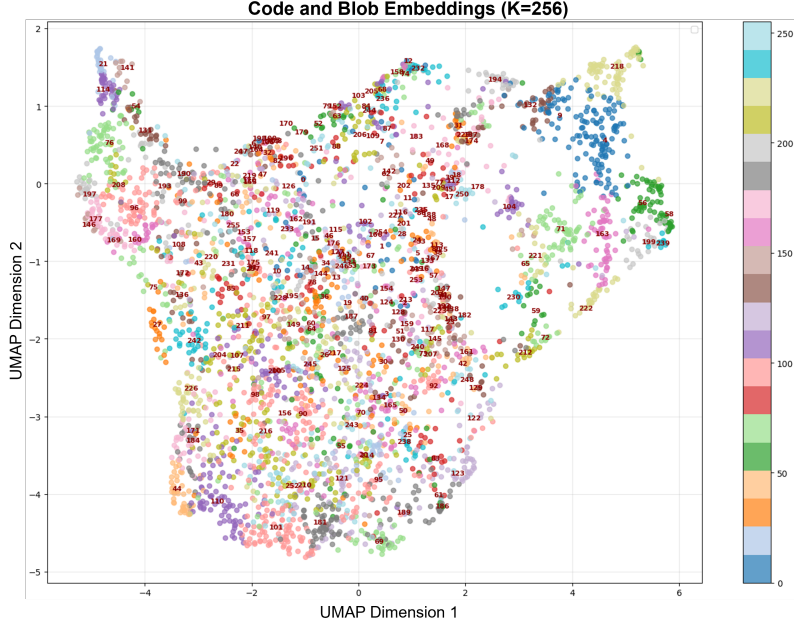


Figure 4: UMAP projection of code and cluster embeddings for EC dataset, random split

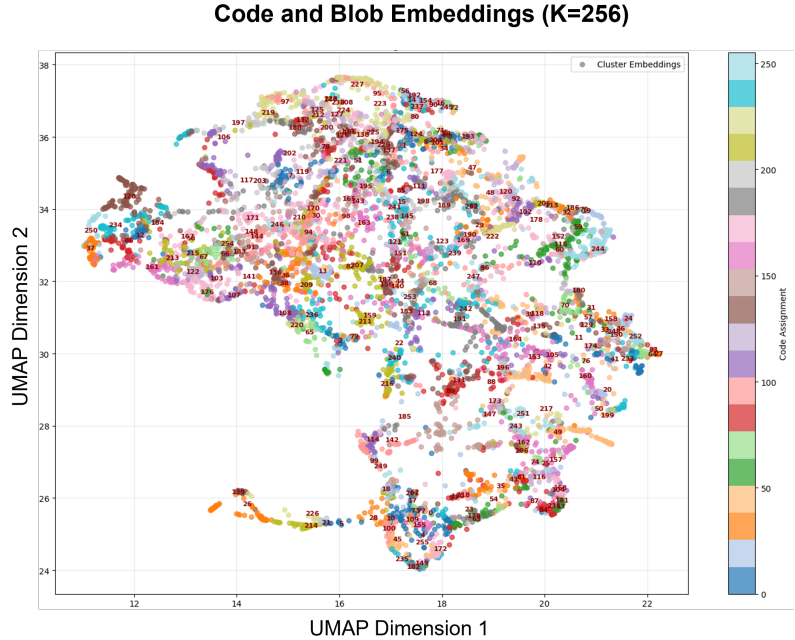


Figure 5: UMAP projection of code and cluster embeddings for EC dataset, structure split

C.1 EMA update of the codebook

We maintain a vector-quantization codebook $\mathbf{E} = \{\mathbf{e}_k\}_{k=1}^K$ and update it with exponential moving averages (EMA) as in VQ-VAE (Van Den Oord et al., 2017). Let $\mathcal{H} = \{\mathbf{h}_s\}$ be the set of cluster embeddings in a minibatch, and let $r_{s,k} \in \{0, 1\}$ denote the hard assignment of \mathbf{h}_s to code k (or soft responsibilities in a soft variant). Define the batch counts and sums

$$n_k = \sum_s r_{s,k}, \quad \mathbf{u}_k = \sum_s r_{s,k} \mathbf{h}_s.$$

With decay $\lambda \in (0, 1)$, EMA keeps running totals \hat{N}_k and $\hat{\mathbf{U}}_k$:

$$\hat{N}_k^{(t)} = \lambda \hat{N}_k^{(t-1)} + (1 - \lambda) n_k, \quad \hat{\mathbf{U}}_k^{(t)} = \lambda \hat{\mathbf{U}}_k^{(t-1)} + (1 - \lambda) \mathbf{u}_k,$$

and updates each code vector to the normalized running mean

$$\mathbf{e}_k^{(t)} = \frac{\hat{\mathbf{U}}_k^{(t)}}{\hat{N}_k^{(t)} + \varepsilon}.$$

We apply stop-gradient to $\hat{N}_k^{(t)}$ and $\hat{\mathbf{U}}_k^{(t)}$ so that code updates do not backpropagate into the encoder. If the accumulators start at zero, an optional bias correction divides numerator and denominator by $(1 - \lambda^t)$. A small ε prevents division by zero and stabilizes the update when counts are low. In practice, $\lambda \in [0.99, 0.999]$ works well; codes with near-zero effective count can be reinitialized to recent cluster embeddings to avoid dead entries. The EMA path replaces direct gradient descent on \mathbf{E} and tracks the empirical means of assigned embeddings with lower variance when assignments fluctuate.